Available online at www.sciencedirect.com
ScienceDirect
Trans. Nonferrous Met. Soc. China 29(2019) 831−839
Transactions of Nonferrous Metals Society of China
www.tnmsc.cn

Feasibility of using recycled CRT funnel glass as partial replacement of high density magnetite sand in radiation shielding concrete

Hua-liang LIU[1,2], Jian-jun SHI[1,2], Hui-qiong QU[3], De-xin DING[1,3]

1. School of Resources and Safety Engineering, Central South University, Changsha 410083, China;
2. School of Civil Engineering, University of South China, Hengyang 421001, China;
3. School of Nuclear Resources Engineering, University of South China, Hengyang 421001, China

Received 7 September 2018; accepted 20 January 2019

Abstract: The recycled cathode ray tube (CRT) funnel glass was used as replacement of magnetite sand in the concrete, and its mass replacement rates were 0, 20%, 40% and 60%, respectively. The flowability, apparent density and mechanical properties of the radiation shielding concrete were investigated, while its γ-ray radiation shielding parameters such as linear and mass attenuation coefficients (μ and μ_m, respectively), thickness values of half-value layer (h_{HVL}) and tenth-value layer (h_{TVL}) were obtained by theoretical calculation, experiment and Monte−Carlo N-Particle (MCNP) simulation code. The experimental results show that the flowability of the concrete increases significantly, whilst its apparent density, compressive strength and static elastic modulus decrease slightly. The calculated, simulated and experimental μ_m, μ, h_{HVL} and h_{TVL} values of all concrete samples are very consistent at the same γ-ray photon energy, and it is feasible to use MCNP code to simulate γ-ray radiation shielding parameters of materials. The calculated results show that in a wide range of γ-ray photon energy, the μ_m value of the concrete with CRT funnel glass replacing magnetite sand is improved effectively, and its radiation shielding performances are the same as those of the control concrete (M−1). By comprehensively comparing the flowability, mechanical properties and γ-ray radiation shielding properties, the concrete samples with 20%−40% funnel glass as fine aggregate have good performances.

Key words: cathode ray tube; funnel glass; concrete; γ-ray; radiation shielding; mechanical properties; Monte−Carlo N-Particle simulation

1 Introduction

A large number of cathode ray tubes (CRTs), which account for over 70% of global e-waste sets [1,2], are eliminated each year as a result of update and replacement of display products. Based on the United Nations University (UNU) statistics, the global generation of e-waste was around 41.8 Mt, the waste CRTs accounted for about 6.3 Mt in 2014, to which Asia contributed 2.5 Mt, and the global e-waste production is expected to increase up to 50 Mt in 2018 [3]. In China, thanks to "Old for new" policy, 5.6×10^7 units of waste electrical appliances in which CRT monitor accounted for 80% were recycled and dismantled in 2010 [4], and approximately 6.0×10^7 waste CRT monitors were discarded in 2012 [5]. According to White Paper on Waste Electrical and Electronic Equipment (WEEE) Recycling Industry in China, as 3.7×10^7 waste computer sets and 3.2×10^7 waste television sets were abandoned, more than 43 Mt of CRT glasses were generated in 2013 [6].

It is estimated that CRT occupies around 65% mass of a television or computer monitor and is constituted of 85% glass, in which a front panel for screen contributes 65%, a back neck for enveloping the electron gun, 5%, and a funnel for connecting the panel and the neck, 30% [7−9]. The CRT glass can be divided into low lead glass and high lead glass according to its lead oxide content, the panel containing 0–3 wt.% lead oxide belongs to the former type, while the funnel and neck for shielding harmful radiation respectively containing 22−25 wt.% and ~30 wt.% lead oxide belong to the latter [10,11]. Heavy metals such as lead and zinc have significant toxic effects and risks on most biological organisms (including human beings) and ecological

Foundation item: Project (14JJ2083) supported by the Natural Science Foundation of Hunan Province, China; Project (2015JC3090) supported by the Science and Technology Department of Hunan Province, China
Corresponding author: De-xin DING; Tel: +86-734-8281781; E-mail: dingdxzzz@163.com
DOI: 10.1016/S1003-6326(19)64993-9

environments [12,13], and the pollution of heavy metals poses great threat to the environment and human beings due to its characteristics of persistence, non-degradability and bioaccumulation [14]. So, the waste CRT is classified as hazardous waste in European Waste Catalogue 2002 and China National Hazardous Waste List 2016 since it contains 22%−28% highly toxic metal lead as well as other high metals such as barium and strontium [15]. Therefore, any inappropriate handling and disposal of CRT waste glass will pose a considerable threat to the environment as well as humanity [11,16].

Generally, closed-loop and open-loop recycling process systems are adopted in the recycling of CRTs [16,17]. The closed-loop process system refers to the recycling of CRTs by sending waste CRTs to CRT factories to obtain lead and lead-free glasses required for manufacturing new CRTs in the manufacturing chain itself [18−20]. The open-loop process system mainly involves the recycling and utilization of CRT glass in the manufacture of new products. Without considering its toxic components, alternative applications for secondary CRT glass have been processed to bricks, decorative tile, nuclear waste encapsulation, construction aggregates, fluxing agent, and sandblasting medium [19,21−28]. However, it is estimated that only about 26% of the discarded CRTs are recycled while the remaining 59% are landfilled due to the lack of satisfied recycling approaches globally [29]. The existing technology of recovering lead from waste CRT glass is not sophisticated, which has disadvantages such as high energy consumption, low recovery efficiency and possible environmental pollution [30−32]. Thus, the disposal of waste CRT glass is becoming an urgent problem to be solved [33]. Meanwhile, concrete material has been widely used in construction, and the aggregate accounts for 60%−75% of the volume of concrete. Due to huge demand for fine aggregate, the natural river sand in China has nearly been exhausted [34], so, CRT funnel glass has been studied as a replacement for natural sand as fine aggregate in mortar or concrete by many researchers [27−29,33−40].

Heavyweight concrete with a density higher than 2600 kg/m^3 is a traditional radiation shielding concrete which uses high density minerals such as barite and magnetite as its aggregate, and has consumed a lot of precious high density minerals. Meanwhile, recycled CRT funnel glass with a density of ~3000 kg/m^3 can be used as a potential high density material for the production of heavyweight concrete. In this work, in order to explore the feasibility of using the hazardous waste CRT funnel glass to replace the high density magnetite sand in the radiation shielding concrete, the recycled ground CRT funnel glass aggregate was used to replace part of high density magnetite sand as fine aggregate in the concrete, and the studies for the fresh, mechanical and radiation shielding behaviors of the concrete were carried out.

2 Experimental

2.1 Materials

2.1.1 Cementitious materials

The cementitious materials consist of Hunan Shaofeng Brand ordinary P·O 42.5 cement and class II low-calcium fly ash. The ordinary cement had a density of 3.11g/cm^3 and specific surface area of 288 m^2/kg, and the fly ash made in Hunan Xiangtan Power Plant, had a density of 2.33 g/cm^3 and specific surface area of 383 m^2/kg.

2.1.2 Aggregate

The local pebbles with an apparent density of 2610 kg/m^3 obtained from Xiangjiang River in Hengyang City were used as coarse aggregate, while nature magnetite sand mixture and ground CRT funnel glass mixture acquired from a glass factory were used as fine aggregate.

The CRT funnel glasses from a glass factory in Hebei Province, China, were washed, mechanically crushed and ground into four fine sands whose particle sizes were 1.6−3, 0.8−1.6, 0.6−0.8 and 0.3−0.6 mm (see Fig. 1), and the mixture that was mixed with four CRT funnel fine sands by mass ratio of 1:2:4:3, belongs to medium sand with a fineness modulus of 2.99 and an apparent density of 2980 kg/m^3.

The magnetite sands with particle sizes distributing from 0−0.25 and 0.25−0.5 to 0.5−1 mm, were the raw materials for the radiation protection of a nuclear power plant. The mixture that was mixed with three magnetite sands by mass ratio of 5:3:2, also belongs to medium sand with a fineness modulus of 2.76 and an apparent density of 4280 kg/m^3.

Fig. 1 CRT funnel glasses with different particle sizes

2.2 Mix proportion and sample preparation

The replacement rates (mass percentage) of the fine CRT funnel glass aggregate for the magnetite sand were set to 0, 20%, 40% and 60%, respectively. The details of mix proportions used in this work are shown in Table 1. The designed strength of the concrete is C30.

The components of the concrete mixture were calculated by mass. Firstly, cementitious materials, fine and coarse aggregates were premixed with 1/2 the mixing water for 3 min. Secondly, the remaining mixing water was added into the mixer, which was mixed for another 3 min. At the end of mixing, a variety of tests were conducted immediately to determine fresh properties of the concrete. Then, the fresh concrete mixture was cast into different types of steel moulds and compacted on a mechanical vibrating table. Finally, the samples were covered with a thin plastic sheet and stored in a laboratory environment at (23±3) °C for 24 h. After that, the concrete samples were demoulded and water-cured at (23±2) °C until the age of testing.

2.3 Test methods

2.3.1 Flowability

The slump test was used to determine the flowability of the fresh concrete mixture according to GB/T 50080. A higher slump value of the mixture indicates a higher flowability.

2.3.2 Apparent density

The apparent density of the concrete was determined by using the method described in GB/T 50080.

2.3.3 Compressive strength

The compressive strength test was conducted on the 3rd, 7th, 28th and 90th day by using a universal testing machine according to GB/T 50081. Three 150 mm × 150 mm × 150 mm cube specimens for each mix proportions in Table 1 were tested and the recorded test results are the average of measurements.

2.3.4 Static elasticity modulus

The static elasticity modulus of the concrete samples was determined on the 28th day by the method described in GB/T 50081. Three 150 mm × 150 mm × 300 mm prismatic samples for each mix proportion were tested and the recorded test results are the average of three measurements.

2.3.5 γ-ray radiation shielding calculation, simulation and test

The linear attenuation coefficient (μ) depends on density of the medium, atomic number of the elements and energy of incident photon, while the mass attenuation coefficient (μ_m) does not depend on the medium density [41−45]. They can be derived from transmission factor curve through fitting Lambert law described by the following equations [41−45]:

$$N=N_0\exp(-\mu X) \quad (1)$$

$$\mu_m=\mu/\rho \quad (2)$$

where N_0 is the dose rate of γ-ray without concrete shielding; N is the dose rate of γ-ray through the concrete sample; X is the thickness of the concrete sample; ρ is the density of the concrete.

The half-value layer thickness (h_{HVL}) and tenth-value layer thickness (h_{TVL}) are defined as the concrete thickness which reduces photon intensity to half and tenth of its initial value, respectively, and can be obtained through theoretical calculation by the following formulas [41−45]:

$$\Delta_{1/2}=\ln(2/\mu) \quad (3)$$

$$\Delta_{1/10}=\ln(10/\mu) \quad (4)$$

where $\Delta_{1/2}$ is the h_{HVL} value; $\Delta_{1/10}$ is the h_{TVL} value.

The calculated γ-ray mass attenuation coefficients of the concrete samples for desired energies from 1 keV up to 100 GeV were obtained by the well-known XCOM program, and the calculated values of μ, h_{HVL} and h_{TVL} were acquired by Formulas (1), (3) and (4), respectively. Then, the simulated γ-ray linear attenuation coefficients of the concrete samples at γ-ray energies of 0.356, 0.662, 1.333, 3 and 5 MeV were obtained by Monte−Carlo N-Particle (MCNP) simulation code, and then the simulated values of μ_m, h_{HVL} and h_{TVL} were calculated using the same above calculation formulas.

The γ-ray radiation shielding test of the concrete was carried out in a specifically designed laboratory apparatus. The test apparatus includes ^{137}Cs and ^{60}Co radiation sources, a γ-ray collimator, and a DM−01

Table 1 Mix proportions of concrete

Specimen	Replacement rate/%	Mass of cementitious material/kg		Mass of fine aggregate/kg		Mass of coarse aggregate pebble/kg	Mass of water/kg
		Cement	Fly ash	CRT	Magnetite sand		
M−1	0	336	84	0	700	1092	188
M−2	20	336	84	140	560	1092	188
M−3	40	336	84	280	420	1092	188
M−4	60	336	84	420	280	1092	188

portable (X-γ) radiation dose rate meter as a detection instrument. The apparatus is shown in Fig. 2. Each group has two samples, and the sample size is 300 mm × 250 mm × 100 mm. Firstly, the dose rate N_0 of γ-ray without concrete shielding was examined. Then, the dose rate N of γ-ray through the concrete sample was measured. Finally, the linear attenuation coefficient (μ), half-value layer thickness (h_{HVL}) and tenth-value layer thickness (h_{TVL}) of the concrete samples with different mix proportions were obtained through theoretical calculation by formulas (1), (3) and (4), respectively [44,45]. The recorded results were the average values of two specimens. The larger the μ value is, the smaller the h_{HVL} and h_{TVL} values will become and the better the anti-radiation performance of the concrete will be.

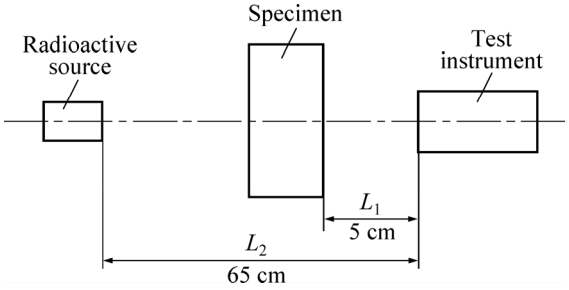

Fig. 2 Schematic of apparatus for measuring γ-ray radiation shielding effectiveness

3 Results and discussion

3.1 Flowability and apparent density

Table 2 shows the effect of replacement level of fine CRT funnel glass aggregate on the slump and apparent density of the concrete. It can be seen from Fig. 3 that the slump height increases gradually with the replacement level of the fine CRT funnel glass aggregate. When the fine magnetite aggregates are replaced by 20%, 40%, and 60% CRT funnel glass aggregates, the slump height increases by 10%, 60%, and 70%, respectively, in comparison with the control concrete (Specimen M−1). The improvement in the fluidity of the fresh concrete mixtures can be caused by the impermeable, lower water absorption and smooth surface of the glass [46].

It can be seen from Fig. 4 that the apparent density decreases with the increase of replacement level of the fine CRT funnel glass aggregate. When the fine magnetite aggregates are replaced by 20%, 40%, and 60% CRT funnel glass aggregate, the apparent density decreases by 0.95%, 2.98%, and 4.73%, respectively, in comparison with the control concrete (Specimen M−1). The reason for this may be that the apparent density of CRT funnel glass as fine aggregate substitute is lower than that of the magnetite fine aggregate replaced by CRT glass.

Table 2 Replacement rate of fine CRT funnel glass aggregate on slump height and apparent density of concrete

Specimen	Replacement rate/%	Slump height/mm	Apparent density/(kg·m^{-3})
M−1	0	30	2750
M−2	20	33	2724
M−3	40	48	2668
M−4	60	51	2620

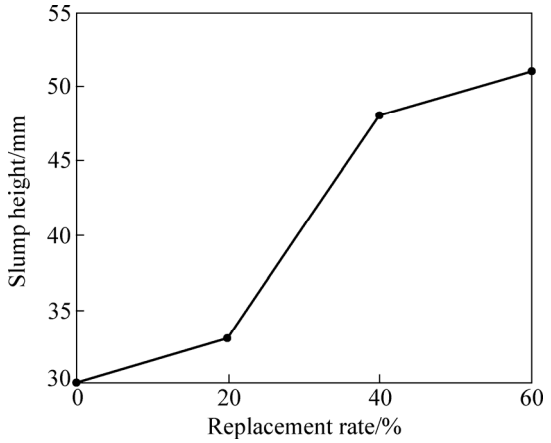

Fig. 3 Relationship between slump height of concrete and replacement rate of fine CRT funnel glass aggregate

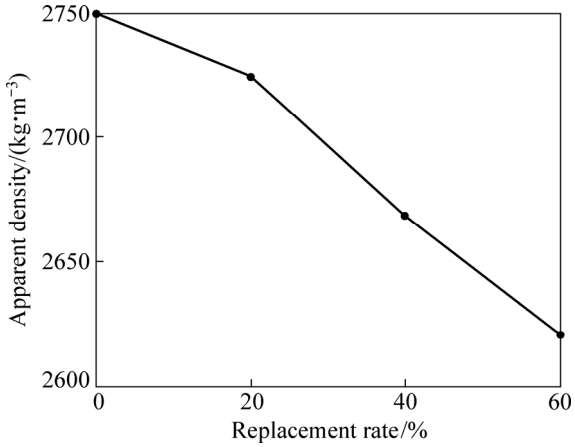

Fig. 4 Relationship between apparent density of concrete and replacement rate of fine CRT funnel glass aggregate

3.2 Mechanical properties

3.2.1 Compressive strength

The compressive strength of the concrete samples with different contents of CRT funnel glass aggregate on the 3rd, 7th, 28th, and 90th day is shown in Fig. 5. It can be seen that compressive strength of the concrete increases steadily with prolonging time. Figure 6 shows the influence of the replacement rate of fine CRT funnel glass aggregate on the compressive strength of the concrete on the 28th day, and it indicates that the compressive strength of concrete on the 28th day decreases with the increase of the replacement rate of

fine CRT funnel glass aggregate. When the replacement rate of fine CRT funnel glass aggregate for magnetite sand varies from 0 to 20%, 40% and 60% in the concrete, the compressive strength decreases from 39.09 to 38.16, 36.66 and 34.12 MPa, with the reduction in the compressive strength of the concrete being 2.4%, 6.2% and 12.7%, respectively, in comparison to the control concrete (Specimen M−1). The reason for the decrease of the mechanical performances of the concrete is that the strength of CRT funnel glass aggregate is less than that of the magnetite aggregate. Also, the smooth surface of CRT funnel glass aggregate affects its binding with cement paste. In addition, due to the Pb leaching from CRT funnel glass aggregate, the leaching rate of Pb increases with the increase of the replacement rate of CRT funnel glass aggregate, which affects the hydration of the cement.

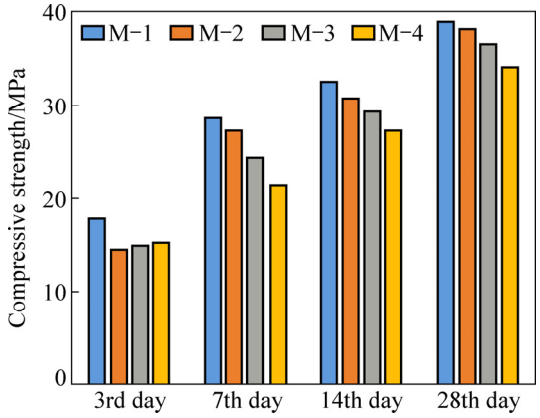

Fig. 5 Compressive strength of concrete samples with different mix proportions on the 3rd, 7th, 14th, and 28th day

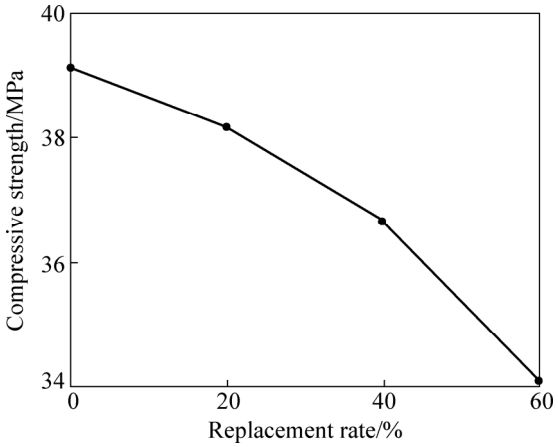

Fig. 6 Relationship between compressive strength and replacement rate of fine CRT funnel glass aggregate on the 28th day

3.2.2 Static elastic modulus

The static elastic modulus of the concrete mixed with different CRT funnel glass contents on the 28th day is shown in Fig. 7. It can be seen that, the static elastic modulus of concrete decreases with the increase of the replacement rate of CRT funnel glass aggregate. With increasing the replacement levels of CRT funnel glass aggregate for magnetite sand from 0 to 20%, 40% and 60% in the concrete, the static elastic moduli decrease from 31.2 to 30.5, 29.2 and 27.7 GPa, and the reductions in the static elastic modulus of the concrete are 2.2%, 6.4% and 11.2%, respectively, in comparison with the control concrete (Specimen M−1). This is mainly due to the poor adhesion between the smooth surface of the CRT funnel glass aggregate and the cement slurry.

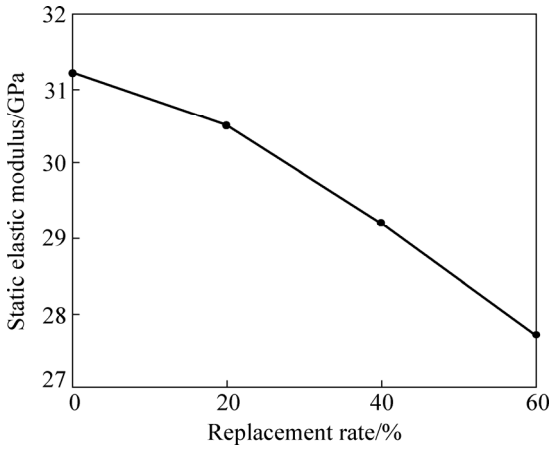

Fig. 7 Relationship between static elastic modulus and replacement rate of fine CRT funnel glass aggregate on the 28th day

3.3 γ-ray radiation shielding performance

Figure 8 shows the variation curves of the calculated γ-ray mass attenuation coefficients of different concretes at various energies calculated by XCOM program, as well as the variation of the simulated values calculated by MCNP code at γ-ray energies of 0.356, 0.662, 1.333, 3 and 5 MeV. As shown in Fig. 8, the XCOM and MCNP calculated results at γ-ray energies of 0.356, 0.662, 1.333, 3 and 5 MeV are very consistent.

In order to compare the effect of replacement rate of CRT funnel glass aggregate on the mass attenuation coefficient of concrete, the mass attenuation coefficient growth factor T is introduced, and its value is equal to

$$T=\frac{\mu_{mi}-\mu_{mc}}{\mu_{mc}}\times 100\% \quad (5)$$

where μ_{mi} refers to the mass attenuation coefficient of concrete sample i calculated by XCOM program at a given photon energy, while μ_{mc} refers to the mass attenuation coefficient of control concrete (M−1) calculated by XCOM program at a given photon energy.

Figure 9 shows the variation law of the mass attenuation coefficient growth factor T of different concrete samples at various photon energies. As can be

seen from Fig. 9, the growth factor curve can be divided into four sections. In the regions where the photon energies are 0.001−0.0018 and 0.0071−0.0152 MeV, the growth factor T is negative, while in the regions where the photon energies are 0.0018−0.0071 and 0.0152−100000 MeV, the growth factor T is positive. The negative growth factor is distributed in the region where the photon energy is very small (the photon energy is less than 0.0152 MeV), and the distribution region is very narrow, which can be basically ignored. In the two regions of photon energies of 0.0018−0.0071 and 0.0152−1 MeV, the positive growth factor values are large, with a maximum value reaching 40%, while in the region of 1−100000 MeV, the positive growth factor values are small. In conclusion, it can be seen from Fig. 9 that replacing high density magnetite sand in concrete with funnel glass can improve the γ-ray mass attenuation coefficient of concrete under a wide range of photon energies.

Table 3, 4, 5 and 6 are used to list the calculated, simulated and experimental μ_m, μ, h_{HVL}, and h_{TVL} values of the concrete samples at γ-ray energies of 0.662 and 1.333 MeV, respectively. It can be seen from these tables that the calculated, simulated and experimental values of all radiation shielding parameters are very consistent at the same photon energy. By comparing the simulated values with the calculated values, the relative error of the mass attenuation coefficient at photon energy of 0.662 MeV is the largest, which is 7.19%, whilst comparing the experimental values with the calculated values, the relative error of h_{HVL} at photon energy of 0.662 MeV is the largest, which is 9.97%.

Figures 10(a) and (b) show the effect of replacement rate of funnel glass on μ_m and μ values of concrete samples at γ-ray energies of 0.662 and 1.333 MeV, respectively. As can be seen from these tables and figures, the calculated, simulated and experimental μ_m values of the concrete samples at γ-ray energies of 662 and 1.333 MeV increase slightly with the increase of replacement rate of funnel glass, of which their maximum values increase by 2.45%, 12.73%, 9.94%, 0.54%, 1.87% and 2.98%, respectively, compared with that of the control concrete (M−1). At γ-ray energy of 0.662 MeV, the simulated and experimental μ values increase with the increase of replacement rate of funnel glass, and their maximum values increase by 7.58% and 4.86%, respectively, whilst the calculated μ value decreases slightly with the increase of replacement rate of funnel glass, and its minimum value decreases by 1.97%, compared with that of the control concrete (M−1). At γ-ray energy of 1.333 MeV, the calculated, simulated and experimental μ values decrease slightly with the increase of replacement rate of funnel glass, and their minimum values decrease by 4.14%, 2.84% and 1.52%, respectively, compared with that of the control concrete (M−1).

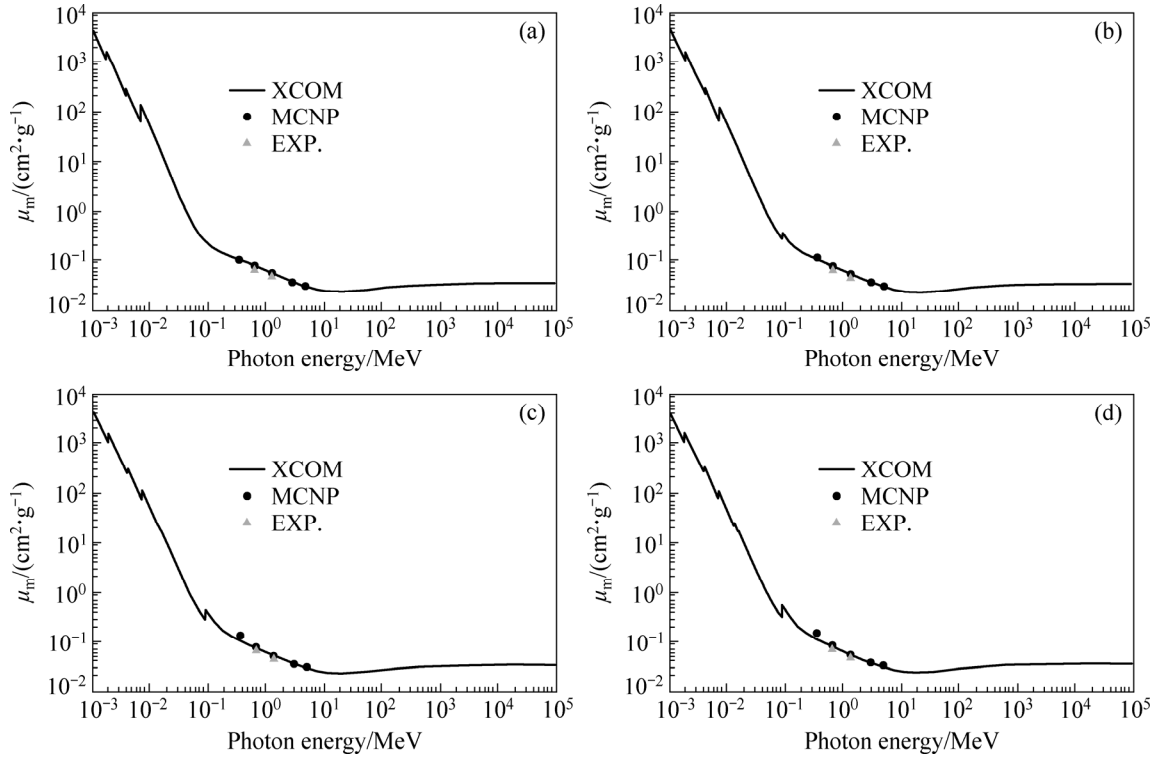

Fig. 8 Calculated, simulated and experimental mass attenuation coefficients for different concrete samples: (a) M−1; (b) M−2; (c) M−3; (d) M−4

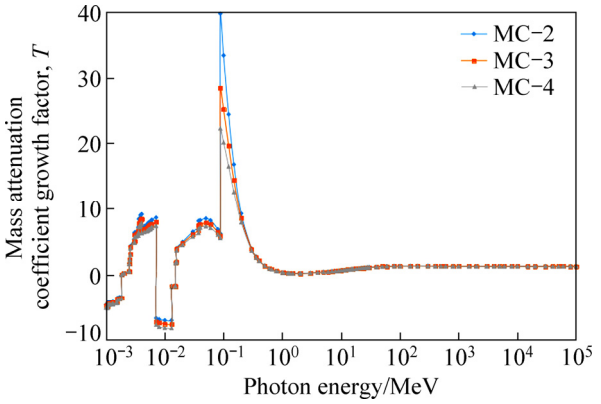

Fig. 9 Variation curves of mass attenuation coefficient growth factor T of concrete samples at various photon energies

Table 3 Calculated, simulated and experimental μ_m values of concrete samples at γ-ray energies of 0.662 and 1.333 MeV

Specimen	μ_m at 0.662 MeV/ ($cm^2 \cdot g^{-1}$)			μ_m at 1.333 MeV/ ($cm^2 \cdot g^{-1}$)		
	XCOM	MCNP	EXP.	XCOM	MCNP	EXP.
M−1	0.0774	0.0754	0.0704	0.0551	0.0535	0.0503
M−2	0.0780	0.0790	0.0731	0.0552	0.0539	0.0507
M−3	0.0787	0.0822	0.0754	0.0553	0.0542	0.0511
M−4	0.0793	0.0850	0.0774	0.0554	0.0545	0.0518

Table 4 Calculated, simulated and experimental μ values of concrete samples at γ-ray energies of 0.662 and 1.333 MeV

Specimen	μ at 0.662 MeV/cm^{-1}			μ at 1.333 MeV/cm^{-1}		
	XCOM	MCNP	EXP.	XCOM	MCNP	EXP.
M−1	0.203	0.198	0.185	0.145	0.141	0.132
M−2	0.202	0.204	0.189	0.143	0.139	0.131
M−3	0.200	0.209	0.192	0.141	0.138	0.130
M−4	0.199	0.213	0.194	0.139	0.137	0.130

Table 5 Calculated, simulated and experimental h_{HVL} values of concrete samples at γ-ray energies of 0.662 and 1.333 MeV

Specimen	h_{HVL} at 0.662 MeV/cm			h_{HVL} at 1.333 MeV/cm		
	XCOM	MCNP	EXP.	XCOM	MCNP	EXP.
M−1	3.41	3.50	3.75	4.79	4.93	5.25
M−2	3.44	3.39	3.67	4.86	4.98	5.29
M−3	3.46	3.31	3.61	4.92	5.02	5.33
M−4	3.49	3.25	3.57	4.99	5.07	5.33

Table 6 Calculated, simulated and experimental h_{TVL} values of concrete samples at γ-ray energies of 0.662 and 1.333 MeV

Specimen	h_{TVL} at 0.662 MeV/cm			h_{TVL} at 1.333 MeV/cm		
	XCOM	MCNP	EXP.	XCOM	MCNP	EXP.
M−1	11.33	11.62	12.45	15.91	16.38	17.44
M−2	11.42	11.28	12.18	16.14	16.53	17.58
M−3	11.49	11.01	11.99	16.35	16.69	17.71
M−4	11.58	10.80	11.87	16.57	16.84	17.71

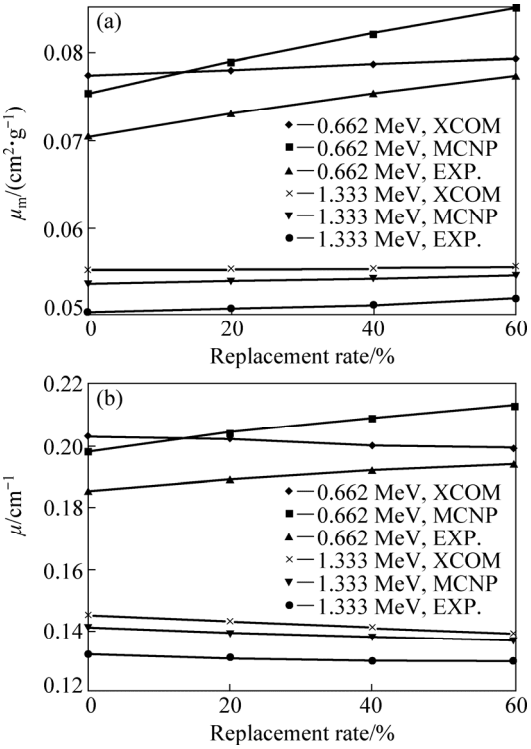

Fig. 10 γ-ray radiation shielding performances of concretes with different replacement rates of fine CRT funnel glass aggregate at γ-ray energies of 0.662 and 1.333 MeV: (a) μ_m; (b) μ

In general, after replacing magnetite with funnel glass at different replacement rates, the new concrete samples still have almost the same γ-ray radiation shielding performances as the control concrete (M−1). Therefore, it is feasible to replace high density mineral aggregates with funnel glass in radiation shielding concrete.

4 Conclusions

(1) The recycled CRT funnel glass with the great advantage of improving radiation shielding properties can be considered as a valuable material not as a waste material. The utilization of the recycled fine CRT funnel glass aggregate replacing high density magnetite sand in radiation shielding concrete is feasible which can be used in nuclear power plants, health care facilities for radiotherapy, nuclear research facilities and storage/ transport containers for radioactive waste, and will save a lot of high density minerals.

(2) With the increase of the replacement rate of fine CRT funnel glass, the flowability of concrete increases significantly, whilst its apparent density, compressive strength, and static elastic modulus decrease slightly. The reductions in compressive strength and static elastic modulus of all the concrete samples are less than 13.5%,

which means that the concrete still has good mechanical properties.

(3) The calculated, simulated and experimental μ_m, μ, h_{HVL}, and h_{TVL} values of all concrete samples are very consistent at the same photon energy, which means that the XCOM program and MCNP code can effectively calculate and simulate the γ-ray radiation shielding performances of materials. In a wide range of γ-ray photon energy, replacing magnetite with funnel glass in the concrete can effectively improve the mass attenuation coefficient. Replacing magnetite sand with funnel glass in the concrete still has almost the same γ-ray radiation shielding performances, compared with the control concrete (Sample M−1).

(4) The comprehensive comparison of flowability, mechanical properties and γ-ray radiation shielding performance shows that the concretes with 20%−40% fine funnel glass aggregates have good performances.

References

[1] GABLE C, SHIREMAN B. Computer and electronics product stewardship: Are we ready for the challenge [J]. Environmental Quality Management, 2010, 11(1): 35−45.

[2] MUELLER J R, BOEHM M W, DRUMMOND C. Direction of CRT waste glass processing: Electronics recycling industry communication [J]. Waste Management, 2012, 32(8): 1560−1565.

[3] BALDÉ C, WANG F, KUEHR R, HUISMAN J. The global e-waste monitor–2014 [R]. Bonn: United Nations University, 2015.

[4] SONG Qing-bin, WANG Zhil-shi, LI Jin-hui, ZENG Xian-lai. Life cycle assessment of TV sets in China: A case study of the impacts of CRT monitors [J]. Waste Management, 2012, 32(10): 1926−1936.

[5] MENG Wen, WANG Xiao-yan, YUAN Wen-yi, WANG Jing-wei, SONG Guang-han. The recycling of leaded glass in cathode ray tube (CRT) [J]. Procedia Environmental Sciences, 2016, 31: 954−960.

[6] China Household Electric Appliances Research Institute. White paper on WEEE recycling industry in China [R]. Beijing: China Household Electric Appliances Research Institute, 2013. (in Chinese)

[7] ANDREOLA F, BARBIERI L, CORRADI A, LANCELLOTTI I. CRT glass state of the art [J]. Journal of the European Ceramic Society, 2006, 27(2): 1623−1629.

[8] HERAT S. Recycling of cathode ray tubes (CRTs) in electronic waste [J]. CLEAN—Soil, Air, Water, 2008, 36(1): 19−24.

[9] MÉAR F, YOT P, CAMBON M, RIBES M. The characterization of waste cathode-ray tube glass [J]. Waste Management, 2005, 26(12): 1468−1476.

[10] LING Tung-chai, POON Chi-sun, LAM Wai-shung, CHAN Tai-po, FUNG K K. Utilization of recycled cathode ray tubes glass in cement mortar for X-ray radiation-shielding applications [J]. Journal of Hazardous Materials, 2011, 199(2): 321−327.

[11] NNOROM I C, OSIBANJO O, OGWUEGBU M O C. Global disposal strategies for waste cathode ray tubes [J]. Resources Conservation & Recycling, 2011, 55(3): 275−290.

[12] FENG Ning-chuan, GUO Xue-yi. Characterization of adsorptive capacity and mechanisms on adsorption of copper, lead and zinc by modified orange peel [J]. Transactions of Nonferrous Metals Society of China, 2012, 22(5): 1224−1231.

[13] SONG Jie, GUO Zhao-hui, XIAO Xi-yuan, MIAO Xu-feng, WANG Feng-yong. Environmental availability and profile characteristics of arsenic, cadmium, lead and zinc in metal-contaminated vegetable soils [J]. Transactions of Nonferrous Metals Society of China, 2009, 19(3): 765−772.

[14] JIANG Bo-feng, SUN Wei-ling. Assessment of heavy metal pollution in sediments from Xiangjiang River (China) using sequential extraction and lead isotope analysis [J]. Journal of Central South University, 2014, 21(6): 2349−2358.

[15] LV Jian-fang, YANG Hong-ying, JIN Zhe-nan, MA Zhi-yuan, SONG Yan. Feasibility of lead extraction from waste cathode-ray-tubes (CRT) funnel glass through a lead smelting process [J]. Waste Management, 2016, 57: 198−206.

[16] JANG Y C, TOWNSEND T G. Leaching of lead from computer printed wire boards and cathode ray tubes by municipal solid waste landfill leachates [J]. Environmental Science & Technology, 2003, 37(20): 4778−4784.

[17] XU Qing-bo, LI Guang-ming, HE Wen-zhi, HUANG Ju-wen, SHI Xiang. Cathode ray tube (CRT) recycling: Current capabilities in China and research progress [J]. Waste Management, 2012, 32(8): 1566−1574.

[18] MOSTAGHEL S, SAMUELSSON C. Metallurgical use of glass fractions from waste electric and electronic equipment (WEEE) [J]. Waste Manag, 2009, 30(1): 140−144.

[19] HREGLICH S, FALCONE R, VALLOTTO M. The recycling of end of life panel glass from TV sets in glass fibres and ceramic productions [M]. London: Thomas Telford Publishing, 2001.

[20] ANDREOLA F, BARBIERI L, CORRADI A, FERRARI A M, LANCELLOTTI I, NERI P. Recycling of EOL CRT glass into ceramic glaze formulations and its environmental impact by LCA approach [M]. International Journal of Life Cycle Assessment, 2007, 12(6): 448−454.

[21] GREGORY J R, NADEAU M C, KIRCHAIN R E. Evaluating the economic viability of a material recovery system: The case of cathode ray tube glass [J]. Environmental Science & Technology, 2009, 43(24): 9245−9251.

[22] DONDI M, GUARINI G, RAIMONDO M, ZANELLI C. Recycling PC and TV waste glass in clay bricks and roof tiles [J]. Waste Management, 2008, 29(6): 1945−1951.

[23] BERNARDO E, ANDREOLA F, BARBIERI L, LANCELLOTTI I. Sintered glass–ceramics and glass–ceramic matrix composites from CRT panel glass [J]. Journal of the American Ceramic Society, 2010, 88(7): 1886−1891.

[24] BERNARDO E, ALBERTINI F. Glass foams from dismantled cathode ray tubes [J]. Ceramics International, 2005, 32(6): 603−608.

[25] LEE Jang-su, CHO Sung-jin, HAN Byung-hyun, SEO Yong-chil, KIM Bo-saeng, HEO S P. Recycling of TV CRT panel glass by incorporating to cement and clay bricks as aggregates [J]. Advances in Biomedical Engineering, 2012, 7: 257−261.

[26] LING Tung-chai, POON Chi-sun. A comparative study on the feasible use of recycled beverage and CRT funnel glass as fine aggregate in cement mortar [J]. Journal of Cleaner Production, 2012, 29−30: 46−52.

[27] SIKORA P, HORSZCZARUK E, RUCINSKA T. The effect of nanosilica and titanium dioxide on the mechanical and self-cleaning properties of waste−glass cement mortar [J]. Procedia Engineering, 2015, 108: 146−153.

[28] LING Tung-chai, POON Chi-sun. Use of recycled CRT funnel glass as fine aggregate in dry-mixed concrete paving blocks [J]. Journal of Cleaner Production, 2014, 68(2): 209−215.

[29] RASHAD A M. Recycled waste glass as fine aggregate replacement in cementitious materials based on Portland cement [J]. Construction & Building Materials, 2014, 72: 340−357.

[30] GONG Yu, TIAN Xiang-miao, WU Yu-feng, TAN Zhe, LV Lei. Recent development of recycling lead from scrap CRTs: A technological review [J]. Waste Management, 2016, 57: 176−186.

[31] OKADA T, NISHIMURA F, YONEZAWA S. Removal of lead from

cathode ray tube funnel glass by combined thermal treatment and leaching processes [J]. Waste Management, 2015, 45: 343−350.
[32] OKADA T, YONEZAWA S. Energy-efficient modification of reduction-melting for lead recovery from cathode ray tube funnel glass[J]. Waste Management, 2013, 33(8): 1758−1763.
[33] YUAN Wen-yi, LI Jin-hui, ZHANG Qi-wu, SAITO F, YANG Bo. Lead recovery from cathode ray tube funnel glass with mechanical activation [J]. Journal of the Air & Waste Management Association, 2013, 63(1): 2−10.
[34] LIU Tie-jun, SONG Wen, ZOU Du-jian, LI Lei. Dynamic mechanical analysis of cement mortar prepared with recycled cathode ray tube (CRT) glass as fine aggregate [J]. Journal of Cleaner Production, 2018, 174: 1436−1443.
[35] ZHAO Hui, POON Chi-sun, LING Tung-chai. Utilizing recycled cathode ray tube funnel glass sand as river sand replacement in the high-density concrete [J]. Journal of Cleaner Production, 2013, 51: 184−190.
[36] LING Tung-chai, POON Chi-sun. Feasible use of recycled CRT funnel glass as heavyweight fine aggregate in barite concrete [J]. Journal of Cleaner Production, 2012, 33(33): 42−49.
[37] SACCANI A, BIGNOZZI M C, BARBIERI L, LANCELLOTTI I, BURSI E. Effect of the chemical composition of different types of recycled glass used as aggregates on the ASR performance of cement mortars [J]. Construction & Building Materials, 2017, 154: 804−809.
[38] LIU Tie-jun, QIN Shan-shan, ZOU Du-jian, SONG Wen. Experimental investigation on the durability performances of concrete using cathode ray tube glass as fine aggregate under chloride ion penetration or sulfate attack [J]. Construction & Building Materials, 2018, 163: 634−642.
[39] INIAGHE P O, ADIE G U. Incorporation of finely ground waste cathode ray tube glass in concrete [J]. Journal of Solid Waste Technology & Management, 2017, 43(3): 207−215.
[40] YAO Zhi-tong, LING Tung-chai, SARKER P K, SU Wei-ping, LIU Jie, WU Wei-hong, TANG Jun-hong. Recycling difficult-to-treat e-waste cathode-ray-tube glass as construction and building materials: A critical review [J]. Renewable & Sustainable Energy Reviews, 2017, 81: 595−604.
[41] EL-KHAYATT A M , ALI A M , SINGH V P. Photon attenuation coefficients of heavy-metal oxide glasses by MCNP code, XCOM program and experimental data: A comparison study [J]. Nuclear Instruments and Methods in Physics Research Section A: Accelerators, Spectrometers, Detectors and Associated Equipment, 2014, 735: 207−212.
[42] BAGHERI R, KHORRAMI MOGHADDAM A, YOUSEFNIA H. Gamma ray shielding study of barium–bismuth–borosilicate glasses as transparent shielding materials using MCNP-4C code, XCOM program, and available experimental data [J]. Nuclear Engineering and Technology, 2017, 49: 216−223.
[43] SAYYED M I, TEKIN H O, KILICOGLU O, AGAR O, ZAIDE M H M. Shielding features of concrete types containing sepiolite mineral: Comprehensive` study on experimental, XCOM and MCNPX results [J]. Results in Physics, 2018, 11: 40−45.
[44] FUGARU V, BERCEA S, POSTOLACHE C, MANEA S, MOANTA A, PETRE I, GHEORGHE M. Gamma ray shielding properties of some concrete materials [J]. Acta Physica Polonica, 2015, 127(4): 1427−1429.
[45] BAGHERI R, MOGHADDAM A K, YOUSEFI A. Gamma-ray shielding study of light to heavyweight concretes using MCNP-4C code [J]. Nuclear Science and Techniques, 2017, 28(2): 1−7.
[46] RASHAD A M. Recycled cathode ray tube and liquid crystal display glass as fine aggregate replacement in cementitious materials [J]. Construction & Building Materials, 2015, 93: 1236−1248.

回收 CRT 锥玻璃部分替代高密度磁铁矿砂在防辐射混凝土中应用的可行性

刘华良[1,2]，石建军[1,2]，屈慧琼[3]，丁德馨[1,3]

1. 中南大学 资源与安全工程学院，长沙 410083；
2. 南华大学 土木工程学院，衡阳 421001；
3. 南华大学 核资源工程学院，衡阳 421001

摘 要：将回收的阴极射线管(CRT)锥玻璃作为辐射屏蔽混凝土中磁铁矿砂的替代材料，其质量替代率分别为 0、20%、40%和 60%。研究此防辐射混凝土的流动性、表观密度和力学性能，同时采用实验、理论计算和蒙特卡洛粒子(MCNP)模拟程序等方法研究混凝土 γ 射线的线性衰减系数(μ)，质量衰减系数(μ_m)、半值层厚度(h_{HVL})和十分之一层厚度(h_{TVL})等辐射屏蔽参数。实验结果表明，混凝土的流动性显著提高，而表观密度、抗压强度和静弹性模量均略微下降。在相同的 γ 射线光子能量条件下，μ_m、μ、h_{HVL} 和 h_{TVL} 等参数的计算、模拟和实验结果吻合较好，这表明用 MCNP 代码模拟材料的 γ 射线辐射屏蔽参数是可行的。计算结果表明，用 CRT 锥玻璃部分代替磁铁矿砂制作的混凝土可以在广泛的 γ 射线光子能量范围内有效地提高 μ_m 值，与对照混凝土(M−1)相比，这种混凝土具有几乎相同的辐射屏蔽性能。对流动性能、力学性能和 γ 射线辐射屏蔽性能的综合比较发现，锥玻璃细骨料替代率为 20%−40%的混凝土具有良好的性能。

关键词：阴极射线管；锥玻璃；混凝土；γ 射线；辐射屏蔽；力学性能；Monte−Carlo 粒子模拟

(Edited by Wei-ping CHEN)